A pH dependent sulfate formation mechanism caused by hypochlorous acid in the marine atmosphere

Liu, Jiarong

Elsevier B.V.
2021-09-15

Liu, J, Ning, A, Liu, L, Wang, H, Kurten, T & Zhang, X 2021, 'A pH dependent sulfate formation mechanism caused by hypochlorous acid in the marine atmosphere', The Science of the Total Environment, vol. 787, 147551. https://doi.org/10.1016/j.scitotenv.2021.147551

http://hdl.handle.net/10138/357778
10.1016/j.scitotenv.2021.147551

A pH dependent sulfate formation mechanism caused by hypochlorous acid in the marine atmosphere

Jiarong Liu[1], An Ning[1], Ling Liu[1], Huixian Wang[2], Theo Kurtén[3*], Xiuhui Zhang[1*]

[1] Key Laboratory of Cluster Science, Ministry of Education of China, School of Chemistry and Chemical Engineering, Beijing Institute of Technology, Beijing 100081, China.

[2] Beijing Guodian Longyuan Environment Engineering Co. Ltd, Beijing 100081, China.

[3] Department of Chemistry, University of Helsinki, Helsinki FI-00014, Finland

* Corresponding authors, E-mail addresses: theo.kurten@helsinki.fi, zhangxiuhui@bit.edu.cn.

Abstract

Secondary sulfate plays a crucial role in forming marine aerosol, which in turn is an important source of natural aerosol at a global level. Recent experimental studies suggest that oxidation of S(IV) compounds, in practice dissolved sulfur dioxide, to sulfate (S(VI)) by hypochloric acid could be one of the most significant pathways for sulfate formation in marine areas. However, the exact mechanism responsible for this process remains unknown. Using high-level quantum chemical calculations, we studied the reaction between dissolved sulfur dioxide and hypochloric acid. We account for the dominant protonation states of reactants in the pH range 3.0-9.0. We also consider possible catalytic effects of species such as H_2O. Our results show that sulfate formation in $HOCl+HOSO_2^-$ and $HOCl+SO_3^{2-}$ reactions relevant to acidic and nearly neutral conditions can occur either through previously proposed Cl^+ transfer or through a novel HO^+ transfer mechanism. In alkaline conditions, where the dominant reactants are OCl^- and SO_3^{2-}, an O atom transfer mechanism proposed in previous experimental studies

may be more important than Cl^+ transfer. Catalysis by common cloud-water species is found to lower barriers of Cl^+ transfer mechanisms substantially. Nevertheless, we find that the dominant S(IV)+HOCl reaction mechanism for the full studied pH range is HO^+ transfer from HOCl to SO_3^{2-}, which leads directly to sulfate formation without $ClSO_3^-$ intermediates. The rate-limiting barrier of this reaction is low, leading to an essentially diffusion-controlled reaction rate. S(IV) lifetimes due to this reaction decrease with increasing pH due to the increasing fractional population of SO_3^{2-}. Especially in neutral and alkaline conditions, depletion of HOCl by the reaction is so rapid that S(IV) oxidation will be controlled mainly by mass transfer of gas-phase HOCl to the liquid phase. The mechanism proposed here may help to explain marine sulfate sources missing from current atmospheric models.

Keywords: Marine aerosol formation; Oxidation pathway; Aqueous phase reaction; DFT studies

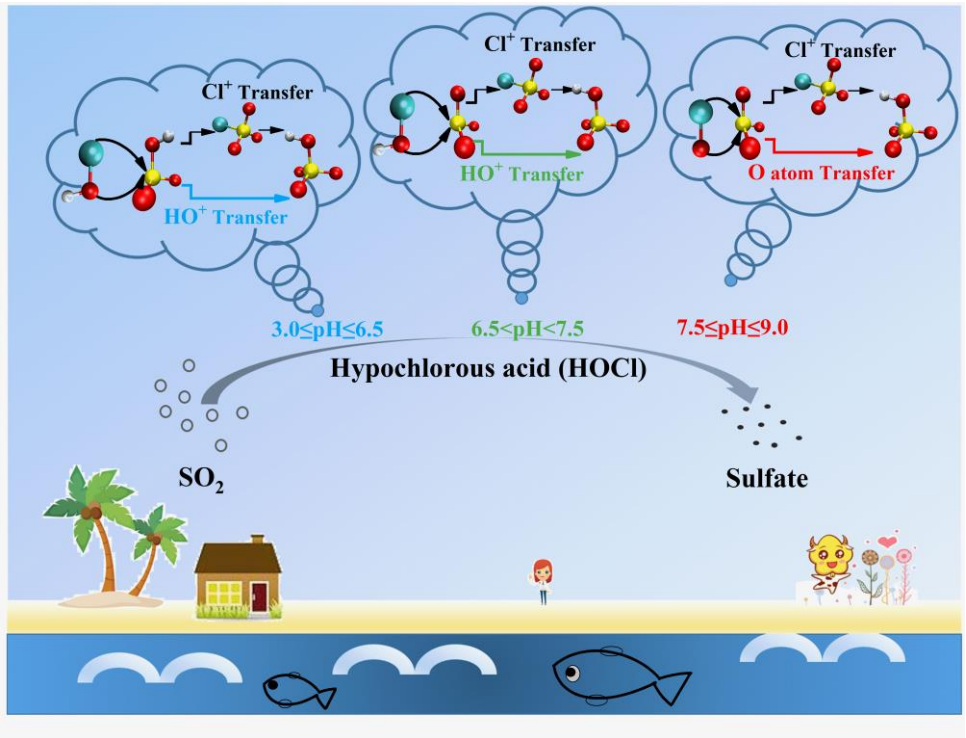

1. Introduction

It is well known that aerosol particles have significant influences on the environment, global climate, and human health(Almeida et al., 2013; Dumka et al., 2020; Ehn et al., 2014; Wang et al., 2015; Zhao et al., 2020). However, there are still some large uncertainties in the estimation of the effects of aerosol particles on all these issues. A major reason for this uncertainty is our poor understanding of the formation process, and therefore the abundance, of aerosol particles especially in marine areas(Choi et al., 2017; Li et al., 2019). Excluding primary sea spray emissions, marine aerosol mainly originates from the secondary formation processes, and is one of the most important sources of natural aerosols at a global level(Dowd et al., 2004; O'Dowd and de Leeuw, 2007; Yan et al., 2020). A series of measurements have shown that the total mass of marine aerosols is dominated by sulfate, with a mass fraction of between 50% and 67%(Choi et al., 2017; Huang et al., 2018). As a predominant component of atmospheric aerosol in general, sulfate is known to have profound impact not only on marine climate, but also on the global climate system(Li et al., 2017; Zhang et al., 2019). On one hand, sulfate aerosol have a direct cooling effect on the radiative balance by efficiently scattering solar radiation(Gen et al., 2019; Huang et al., 2014). On the other hand, sulfate aerosol also act as the potential cloud condensation nuclei (CCN), thus altering the number, size and water uptake of the cloud droplets, and leading to even greater, though highly uncertain, indirect radiative effects(Hung et al., 2018). Measurements have shown that CCN number concentrations dramatically increase following increases of sulfate aerosol(Novakov et al., 1994).

The main source of secondary (non-sea salt) sulfate in marine areas is oxidation of sulfur dioxide (SO_2), which mainly originates from the oxidation of dimethyl sulfide (DMS) emitted by oceanic phytoplankton (Chen et al., 2018; Hung and Hoffmann, 2015; Landim et al., 2018) or from long-range transport of human emissions including fossil fuel combustion and industrial processes(Alexander et al., 2009). The oxidation of SO_2 to sulfate has attracted much interest, and very many studies have been performed to identify the detailed formation process of sulfate in different conditions(Chen et al., 2016; Gen et al., 2019; He et al., 2014; Li et al., 2018; Wang et al., 2016; Wang et al., 2020). Based on model simulations, the main sulfate (S(VI)) formation process in marine areas is thought to be oxidation of dissolved SO_2 ($H_2SO_3 + HOSO_2^- + SO_3^{2-}$) in cloud water. Dissolved SO_2 is often denoted simply as S(IV). This process generally prevails over gas-phase oxidation due to the high relative humidity (RH), and consequent high liquid water content, in typical marine air(Alexander et al., 2012; Chen et al., 2016). The main known oxidation mechanisms of S(IV) in cloud water are its reactions with hydrogen peroxide (H_2O_2), ozone (O_3), nitrogen dioxide (NO_2) and various transition metal ions together with molecular oxygen (O_2)(Alexander et al., 2009; Alexander et al., 2012; Brandt and van Eldik, 1995; Chandler et al., 1988; Clifton et al., 1988; Harris et al., 2013; Hung and Hoffmann, 2015; Kunen et al., 1983; McArdle and Hoffmann, 1983; Shen et al., 2012). All the corresponding oxidation mechanisms are pH dependent, for example due to the pH dependence of the relative concentrations of the three reactant species H_2SO_3, $HOSO_2^-$ and SO_3^{2-}. Although all the above sulfate formation processes have been considered in atmospheric models, marine sulfate

concentrations are still underestimated significantly. This underestimation is often attributed to the existence of some important but as yet unknown pathways for converting S(IV) to sulfate(Cheng et al., 2016; Huang et al., 2014; Wang et al., 2014; Wang et al., 2016; Zheng et al., 2015).

Recent studies have suggested that S(IV) oxidation reaction caused by hypochloric acid(HOCl) in cloud water is a potentially important source of sulfate, as hypochloric acid is present in the marine atmosphere (with reported gas-phase mixing ratios ranging from 5 to 173 pptv), and is well-known to be an efficient oxidant(Alexander et al., 2009; Alexander et al., 2012; Chen et al., 2016; Chen et al., 2017; Keene et al., 1998; Vogt et al., 1996; von Glasow et al., 2002). In particular, Chen *et al*. provided observational evidence for the role of hypochloric acid in sulfate formation in marine areas by a combination of observations and modeling of the oxygen isotope ratio $\triangle^{17}O(nssSO_4^{2-})$(Chen et al., 2016). They found that the oxidation processes of S(IV) by hypohalous acids (HOX =HOCl, HOBr) can contribute from 33 to 50 % of the total sulfate production over the entire area sampled. Similarly, Keene *et al*. determined that reaction with hypochloric acid is the principal oxidation pathway for S(IV) leading to sulfate formation at a pH value of 5.5 using the photochemical box model MOCCA in marine areas(Keene et al., 1998).

Laboratory experiments have also been performed to investigate the dynamics and mechanisms of the corresponding reaction processes. Liu *et al*. directly determined the rate of sulfate formation from the reaction between HOCl and $HOSO_2^-$ in low-pH aerosol particles by measuring the concentration of sulfate as a function of time in a

flow tube. They proposed a possible two-step sulfate formation mechanism involving Cl^+ transfer(Liu and Abbatt, 2020). Fogelman *et al*. obtained the reaction rate constant between HOCl and SO_3^{2-} at near-neutral pH by measuring the loss of reactant per unit time, and also proposed a Cl^+ transfer mechanism(Fogelman et al., 1989). Despite these studies, the speculated pathway for sulfate formation has not been completely identified or verified, because the key chlorosulfate ion ($ClSO_3^-$) intermediate of the Cl^+ transfer mechanism has not been directly characterized in the experiments. Despite the electrostatic repulsion inevitably present between two anions, Fogelman *et al*. found that the $OCl^- + SO_3^{2-}$ reaction can lead to sulfate formation in basic conditions. They proposed that the reaction proceeds via a one-step mechanism involving O atom transfer(Fogelman et al., 1989). Even though the speculated O atom transfer mechanism seems reasonable, the corresponding product has also not been experimentally identified. A Cl^+ transfer mechanism could be possible also in basic conditions, as this mechanism would involve a O^{2-} leaving group, which might have an even greater potential to react spontaneously with H_2O (and thus promote the reaction) than the Cl^- leaving group of the Cl^+ transfer mechanism.

As both dissolved S(IV) and hypochloric acid exist in different protonation states depending on the pH (see Fig. 1 below for details), and the different forms of the reactants are likely to display distinct reaction kinetics, the overall S(IV) + HOCl reaction mechanism is likely to be complex. Furthermore, other molecules, including both water and the product sulfate, may participate in the reaction mechanisms, again depending on the pH. In order to elucidate the overall reaction for S(IV) + HOCl, we

have accordingly used high-level quantum chemical methods to explore several possible sulfate-forming processes for the wide pH range of 3.0-9.0(Fridlind and Jacobson, 2000; Pszenny et al., 2003) relevant to marine areas. We have also probed the catalytic effects of common atmospheric species such as water and sulfate on the S(IV) + HOCl reactions.

2. Methods

Electronic structure calculation. Density functional theory (DFT) calculations were carried out using the Gaussian 16, revision A. 03 programs package(Frisch et al., 2016). The geometry optimizations and vibrational frequency calculations of reactants, products, and transition states were performed at the M06-2X/6-311++G (3df, 3pd) level of theory(Elm et al., 2012; Mardirossian and Head-Gordon, 2016; Zhao and Truhlar, 2008), which has been found to be well suited to compute thermochemistry and barrier heights of molecular systems relevant to the atmosphere(Li et al., 2018; Rong et al., 2020; Zhang et al., 2018; Zhao and Truhlar, 2008). The connection of each transition state to reactants and products was confirmed by intrinsic reaction coordinate (IRC) calculations at the same level of theory. Single point energy corrections were calculated at the CCSD(T)-F12/cc-pVDZ-F12 level of theory with the ORCA 4.10 program, using the geometry optimized at the M06-2X/6-311++G (3df, 3pd) level of theory(Lane and Kjaergaard, 2009; Neese, 2012; Peterson et al., 2008). In addition, the solvent environment was modelled using the continuum solvation model based on solute electron density (SMD) at the M06-2X/6-311++G (3df, 3pd) level of theory(Marenich et al., 2009). SMD is considered to be highly adequate to describe

detailed reaction processes and predict the corresponding reaction free energy barriers in aqueous solutions(Miguel et al., 2016; Ostovari et al., 2018; Xu and Coote, 2019), especially for atmospherically relevant processes(Keshavarz et al., 2021; Minakata et al., 2015). Also, some studies suggest that the SMD-based implicit solvent treatment may even outperform explicit water treatment in predicting free energy barriers of reactions in aqueous environment(Chen et al., 2019). Free energies reported here include solvent corrections, and correspond to a temperature of 298.15K, and a reference concentration of 1 mol/L. The details of the free energy calculations are summarized in Section 1.1 of the SI.

Kinetics calculations. The studied mechanisms involve both (barrierless) complex or intermediate formation steps, and subsequent reactions of these complexes or intermediates. Our kinetics treatment is based on the pseudo-steady-state approach (PSSA), and contains two types of parameters: usually bimolecular equilibrium constants (K_{eq}), and formally unimolecular reaction rate coefficients (k). The latter are calculated in terms of Transition State Theory (TST)(Evans and Polanyi, 1935; Eyring, 1935; Truhlar et al., 1983) ignoring tunneling as the reactions involve heavy-atom transfers. These parameters are calculated as follows:

$$K_{eq}=(c_0)^{\Delta n}\exp\left(-\frac{\Delta G_{eq}}{RT}\right) \quad (1)$$

$$k=\frac{k_B T}{h}\exp\left(-\frac{\Delta G^0}{RT}\right) \quad (2)$$

where ΔG_{eq} is the difference of the Gibbs free energy between the reactant(s) and the product(s) of a reaction, R is the gas constant, T is the temperature, k_B is the Boltzmann constant, h is the Planck constant, c_0 is the reference concentration (1 mol/L) at which

ΔG_{eq} is calculated, and Δn is the change in the number of separate species in the reaction (-1 for the typical case of a bimolecular association reaction where two reactants form a complex or an adduct). Similarly, ΔG^0 is the Gibbs free energy barrier, i.e the difference in the Gibbs free energy between a reactant (usually a reactant complex or adduct) and the transition state.

The bimolecular rate constant for an overall reaction (k_{bim}) involving the formation of an initial complex, which then needs to cross a barrier, is then:

$$k_{bim}=K_{eq}\times k \quad (3)$$

In addition, diffusion limitations should be considered especially for low-barrier or barrierless reactions. Collins-Kimball theory(Collins and Kimball, 1949) was used to calculate the overall rate constants $k_{overall}$ for reactions involving an initial barrierless complex formation:

$$k_{overall}=\frac{k_{bim}\times k_D}{k_{bim}+k_D} \quad (4)$$

Where k_D is the steady-state Smoluchowski rate constant that can be expressed as Eq. (5)(Chang, 2000; Smoluchowski, 1917)

$$k_D=4\pi R D_{AB} N_A \quad (5)$$

where N_A is the Avogadro constant and R denotes the reaction distance. Generally, R is the sum of the radii of two reactants for free diffusion processes. In addition, D_{AB} is the mutual diffusion coefficient of the reactants A and B, computed as the sum of D_A and D_B**(Truhlar, 1985)**, which in turn are calculated by using the Stokes-Einstein approach**(Einstein, 1905; Stokes, 1903)**:

$$D_{A\text{ or }B}=\frac{k_B T}{6\pi\eta a_{A\text{ or }B}} \quad (6)$$

where η is the viscosity of water, and $a_{\text{A or B}}$ is the radius of reactant A or B, which can be estimated, assuming spherical reactants, using the volume of the reactants computed with Gaussian 16, revision A. 03(Frisch et al., 2016). Rates for the barrierless dissociation of complexes were computed by detailed balance as k_D/K_{eq}, with k_D and K_{eq} computed from Eq (5) and Eq (1), respectively.

In addition, it should be noted that, in the present system, reaction might occur between two anions, and thus, the diffusion in a coulomb potential has an R value smaller than that of free diffusion process because of the strong electrostatic repulsion. k_D might then decrease because of the decreased R. In this case, R can be calculated as(Roussel, 1985):

$$R=\frac{Z_A Z_B e^2}{4\pi\epsilon k_B[e^{(\frac{Z_A Z_B e^2}{4\pi\epsilon k_B r})}-1]} \quad (7)$$

where Z_A and Z_B are the charges for the two ions, ϵ is the dielectric constant for water, k_B is Boltzmann's constant, T is the temperature, and r is the sum of radii of the two reactants.

Wavefunction analysis. Wavefunction analysis was carried out at the start of the study to determine the possible reaction mechanisms available to each combination of reactants. The electrostatic potential (ESP) on the molecular van der Waals (vdw) surface is crucial for predicting the potential reaction sites of intermolecular interactions. The site possessing more positive ESP tends to attract the site which possesses more negative ESP, and vice versa**(Manzetti and Lu, 2013; Murray and Politzer, 2011)**. We accordingly calculated the ESP color-mapped isosurface using Multiwfn 3.7**(Lu and Chen, 2012)**, and VMD 1.9.3**(Humphrey et al., 1996)**. Furthermore, the contour

map of electron density difference between transition states and reactant complexes, which can indicate the structural changes in the reaction process, was analyzed using Multiwfn 3.7**(Lu and Chen, 2012)**.

3. Results and discussion

The reactants S(IV) and hypochloric acid exist in different protonation states at different pH, potentially leading to different reaction mechanisms. As shown in Fig. 1, based on measured pK_a values, the S(IV) reactant exists primarily in the form of $HOSO_2^-$ at low (but atmospherically relevant) pH, and in the form of SO_3^{2-} in near-neutral or basic conditions (pH>6.5)(C. Drexler et al., 1992; Kunen et al., 1983). H_2SO_3 is the main form of S(IV) only at a very low pH (pH <1.5)(C. Drexler et al., 1992). Also, this form is extremely unstable(Li and McKee, 1997; Voegele et al., 2002; Voegele et al., 2004). Thus, considering the range of pH from 3.0 to 9.0 in the marine areas, and the instability of H_2SO_3, the corresponding oxidation reactions involving H_2SO_3 were not considered in the present work. In addition, it should be noted that although two bisulfite ion isomers (HSO_3^- and $HOSO_2^-$) have been found in the aqueous phase, only the dominant one with the proton bonded to the oxygen atom has been chosen for the study of oxidation reactions in the present work(Baird and Taylor, 1981; Brown and Barber, 1995; Horner and Connick, 1986). For the hypochloric acid reactant, HOCl is the dominant form at pH <7.5, while OCl^- dominates for pH > 7.5(Shaka et al., 2007). See Section 1.2 of the SI for details. To comprehensively investigate the reaction process of S(IV) oxidation by hypochloric acid, we have considered multiple reactions

mechanisms as suggested by ESP surfaces, involving all the dominant reactant forms for a wide range of pH, as illustrated by Eqs. (8), (9) and (10):

$$3.0 \leq pH \leq 6.5,\ HOSO_2^- + HOCl \rightarrow \text{sulfate} \quad (8)$$

$$6.5 < pH < 7.5,\ SO_3^{2-} + HOCl \rightarrow \text{sulfate} \quad (9)$$

$$7.5 \leq pH \leq 9.0,\ SO_3^{2-} + OCl^- \rightarrow \text{sulfate} \quad (10)$$

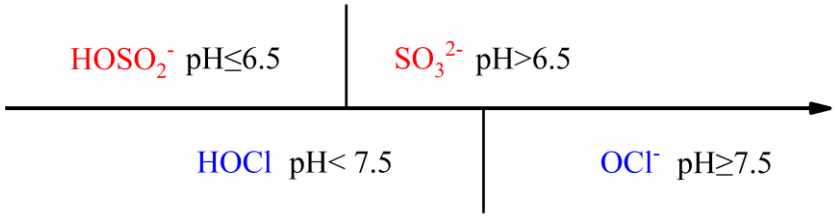

Fig. 1. The dominant forms of reactants S(IV) and hypochloric acid at different ranges of pH in the cloud water.

3.1. Sulfate formation mechanism in weakly acidic water (3.0 ≤ pH ≤ 6.5)

Based on the above analysis, S(IV) and hypochloric acid will be mainly exist as $HOSO_2^-$ and HOCl, respectively, at the typical pH (pH=3.0-6.5) of cloud water. In order to identify the potential reaction sites between $HOSO_2^-$ and HOCl, an in-depth exploration of the ESP on the molecular vdw surface has been performed, and shown in Fig. 2(a). The site which possesses more positive ESP has stronger ability to attract electrophiles, and has a greater ability to react with the site possessing more negative ESP(Lu and Chen, 2012; Manzetti and Lu, 2013; Murray and Politzer, 2011). As illustrated in Fig. 2(a), the chlorine atom (site 2) of HOCl possesses more positive ESP, implying that it has the potential to interact with the sulfur atom (site 1) of $HOSO_2^-$ with negative ESP. Similarly, the oxygen atom (site 3) of HOCl could also interact with the

sulfur atom (site 1) of $HOSO_2^-$, because of the much more negative ESP of site 3 compared to site 1. Thus, based on the ESP surface, there are two potential reaction pathways of $HOSO_2^-$ with HOCl to form sulfate. In addition to the previously proposed Cl^+ transfer mechanism (Pathway 1(acidic))(Liu and Abbatt, 2020), the ESP results suggest that also a hitherto unreported HO^+ transfer mechanism (Pathway 2(acidic)) should be investigated.

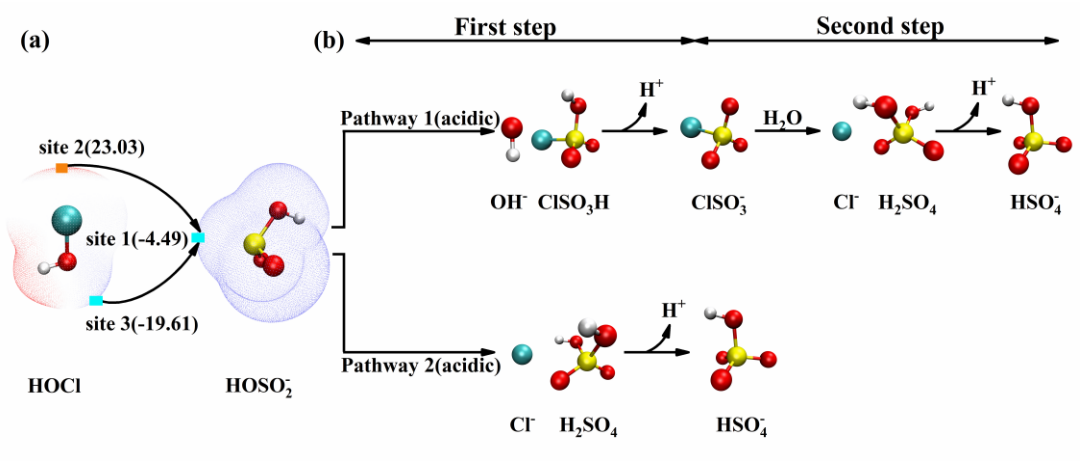

Fig. 2. (a) ESP-mapped molecular vdW surfaces of HOCl and $HOSO_2^-$, in units of kcal/mol. Surface local minima and maxima of ESPs of different functional groups in the corresponding molecules are represented as blue and orange squares, respectively. (b) Two possible pathways for the reaction of $HOSO_2^-$ with HOCl leading to sulfate formation. The white, cyan, red, and yellow spheres represent H, Cl, O, and S atoms, respectively.

The potential energy profiles for the reaction pathways discovered for $HOSO_2^-$ + HOCl are shown in Figs. 3(a) and (b). These figures also show the optimized structures of the reactant complexes (R_{cn}), transition states (TS_n) and product complexes (P_{cn}) for the two studied pathways. As shown in Fig. 3 (a), the reaction of $HOSO_2^-$ with HOCl via Pathway 1(acidic) begins with the formation of reactant complex $HOCl\cdots HOSO_2^-$

(R_{c1}). This complex then crosses a shallow barrier (5.3 kcal/mol relative to the separated reactants) corresponding to TS_1, forming a complex of $ClSO_3H...OH^-$, (denoted P_{c1}). Next, proton transfer forms a $ClSO_3^-...H_2O$ complex (denoted R_{c2}), lowering the free energy by 54.2 kcal/mol. (This complex is bound by 2.8 kcal/mol with respect to separated $ClSO_3^- + H_2O$; not shown in the Fig. 3(a)) The next step on reaction Pathway 1(acidic) is hydrolysis of the $ClSO_3^-$ intermediate. As shown in Fig. 3(a), the $ClSO_3^-...H_2O$ complex (R_{c2}) is connected to a four-membered ring transition state TS_2 (55.3 kcal/mol higher in free energy), where one proton of H_2O transfers to the oxygen atom of $ClSO_3^-$, while the remaining hydroxyl of H_2O binds to the sulfur atom of $ClSO_3^-$. The product of this reaction step is a complex between sulfuric acid and chloride, $H_2SO_4…Cl^-$ (P_{c2}), which is bound by 53.9 kcal/mol with respect to separated H_2SO_4 and Cl^-. Due to the very high free energy of TS_2, this process is not a competitive route for sulfate formation.

However, multiplied hydrogen-bonding species present in cloud water, including water (H_2O), sulfuric acid (H_2SO_4) and bisulfate ions (HSO_4^-), have the ability to catalyze proton transfer reactions(Liu et al., 2015; Meijer and Sprik, 1998; Torrent-Sucarrat et al., 2012). We have investigated the effect of these three species on the hydrolysis of $ClSO_3^-$, and found that all three substantially lower the free energy barrier for the process. The free energy barriers of the catalyzed reactions, relative to the corresponding three-body reactant complexes $ClSO_3^-...H_2O...X$, are 24.3, 25.0, and 23.9 kcal/mol, for X= H_2O, H_2SO_4, and HSO_4^-, respectively. See also Fig. 3(a) and Fig. S1 of the SI. Here, we discuss further the hydrolysis $ClSO_3^-$ catalyzed by H_2O, the most

abundant species in the aqueous environment, as an example of this general catalytic mechanism. As shown in Fig. 3(a), the hydrolysis reaction catalyzed by H_2O proceeds through the clustering of an additional water molecule with $ClSO_3^-…H_2O$ reactant complex (R_{c2}), forming $ClSO_3^-…H_2O…H_2O$ (R_{c3}). Next, R_{c3} can be converted into the product complex $HSO_4^-…H_3O^+…Cl^-$ (denoted P_{c3}), and finally to separated HSO_4^-, H_3O^+, and Cl^-, via a six-membered ring transition state TS_3. The barrier for this catalyzed process is almost 30 kcal/mol lower than that of the uncatalyzed reaction. The reason for this lowering is likely that the strong ring tension of the closed four-membered ring in the uncatalyzed reaction is reduced in the catalyzed reaction, as the ring size is increased by a hydrogen bonding network involving H_2O. The contour maps of the electron density differences between R_{c3} and TS_3 in Fig. S3 illustrate the detailed reaction process. The proton transfer from the reactant H_2O to the oxygen atom of the catalyst H_2O forms a new H-O single bond. The remaining hydroxyl moiety of the reactant H_2O binds to the sulfur atom of $ClSO_3^-$, forming a new S-O single bond. Meanwhile, the chloride ion leaves the sulfur atom of $ClSO_3^-$ through the cleaving of the Cl-S single bond. Sulfate formation from $HOSO_2^-$ + HOCl through the Cl^+ transfer mechanism (Pathway 1(acidic)) proposed in experimental studies(Liu and Abbatt, 2020) is thus feasible, but only with the help of a catalyst such as H_2O.

Moreover, we also discovered an unexpected novel mechanism for $HOSO_2^-$ + HOCl, illustrated by Pathway 2(acidic) in Fig. 3(b). Starting with the reactant complex $HOSO_2^-…HOCl$ (R_{c4}), the reaction goes on to form the product complex $H_2SO_4…Cl^-$ (P_{c4}) through the transition state TS_4. This mechanism involves the direct formation of

sulfate by transferring a HO^+ group from HOCl to $HOSO_2^-$. The free energy barrier of this pathway is 21.2 kcal/mol relative to the separated reactants. We investigated whether also this pathway may be catalyzed by additional hydrogen-bonding molecules. We find that, H_2O, the most abundant molecule in aqueous environment, can form hydrogen-bonded complexes with $HOSO_2^-$, and also with $HOSO_2^-$…HOCl (R_{c4}), leading to a H_2O…$HOSO_2^-$…HOCl reactant complex (R_{c5}). As illustrated in Fig. 3(b), the catalyzed reaction then leads to the formation of a H_3O^+…HSO_4^-…Cl^- product complex (P_{c5}) through transition state TS_5, in which the Cl-O bond of HOCl is cleaved. and an O-S bond between $HOSO_2^-$ and HOCl is formed. The Gibbs free energy barrier of this process is reduced to 19.5 kcal/mol relative to the separated reactants, about 1.5 kcal/mol lower than the uncatalyzed reaction. Thus, H_2O may have a modest catalytic effect also on the HO^+ transfer mechanism (pathway 2(acidic)) discovered here. In addition, we found that products of this pathway, such as H_2SO_4 and HSO_4^-, could also act as catalysts. The corresponding processes are shown in Fig. S2 of the SI.

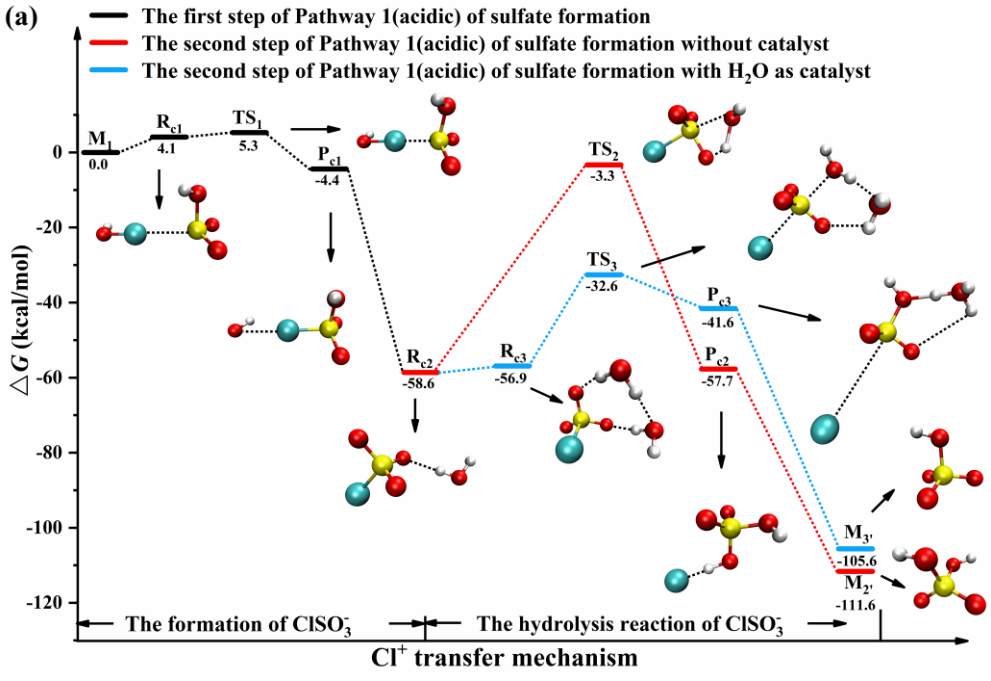

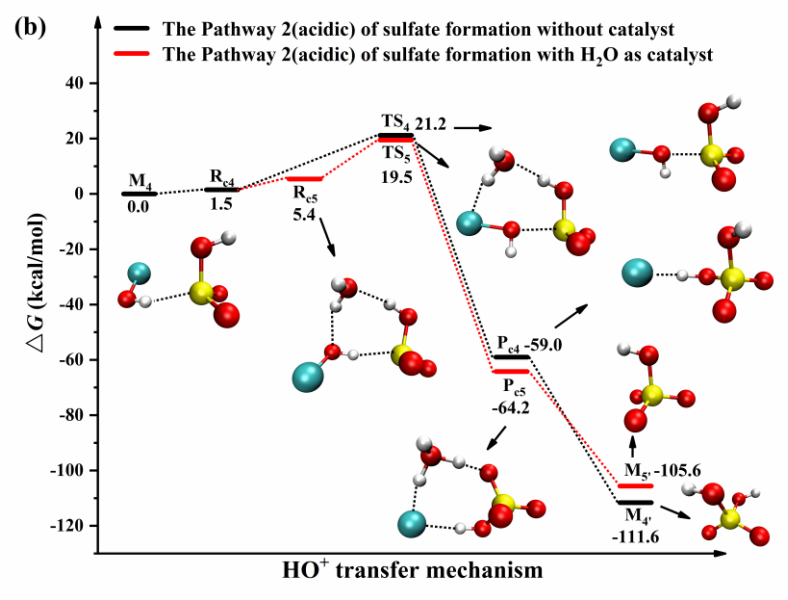

Fig. 3. The Gibbs free energy profile (kcal/mol, at 298.15 K and a reference concentration of 1 mol/L) for the reaction of HOCl with $HOSO_2^-$ through (a) Pathway 1(acidic) and (b) Pathway 2(acidic), at the CCSD(T)-F12/cc-pVDZ-F12//M06-2X/6-311++G (3df, 3pd) level of theory. Solvent corrections are included in the M06-2X calculations using the SMD model. The white, cyan, red, and yellow spheres represent H, Cl, O, and S atoms, respectively.

3.2. Sulfate formation mechanism in neutral water (6.5<pH<7.5)

As pH increases, SO_3^{2-} becomes to the dominant form of S(IV). In neutral cloud water (6.5<pH<7.5), the S(IV) + HOCl reaction thus mainly proceeds through SO_3^{2-} + HOCl. In addition to the Cl^+ transfer mechanism (Pathway 1(neutral)) proposed by earlier experimental studies(Liu and Abbatt, 2020), which is similar to the mechanism in weakly acidic water except for the participation of SO_3^{2-} instead of $HOSO_2^-$, our ESP analysis (see Fig. 4) suggests the existence of a HO^+ transfer mechanism also for SO_3^{2-} + HOCl (Pathway 2(neutral)). According to the ESP analysis, the chlorine atom (site 2) of HOCl possesses positive ESP, enabling it to react with the sulfur atom (site 4) of

SO_3^{2-} with negative ESP. Meanwhile, the oxygen atom (site 3) of HOCl may also react with the sulfur atom (site 4) of SO_3^{2-} because of the much more negative ESP of site 3 compared to site 4.

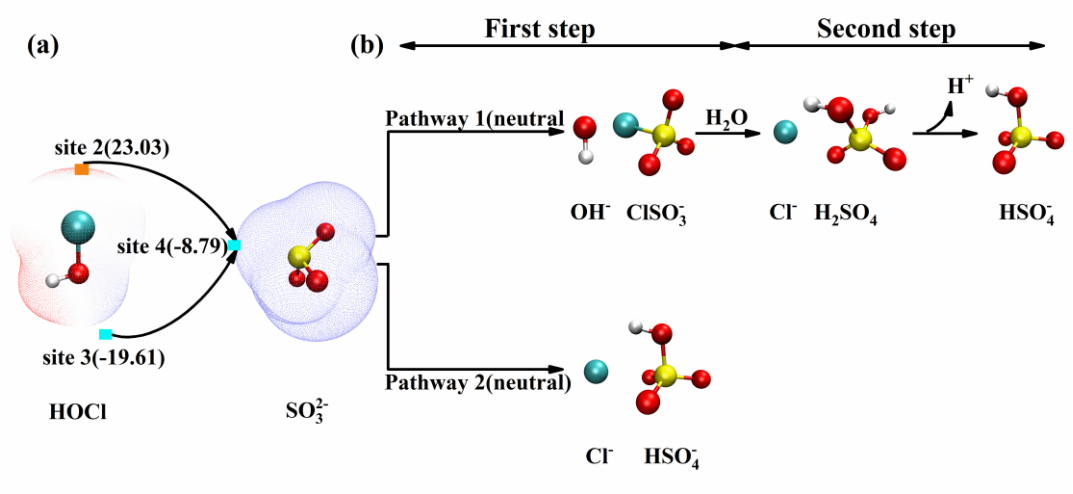

Fig. 4. (a) ESP-mapped molecular vdW surface of HOCl and SO_3^{2-}, in units of kcal/mol. Surface local minima and maxima of ESPs of different functional groups in the corresponding molecules are represented as blue and orange squares, respectively. (b) Two possible reaction pathways for the reaction of SO_3^{2-} with HOCl leading to sulfate formation. The white, cyan, red, and yellow spheres represent H, Cl, O, and S atoms, respectively.

The potential energy profiles of Pathway 1(neutral) and Pathway 2(neutral) as well as the corresponding geometries on the reaction path are shown in Figs. 5(a) and (b), respectively. In Pathway 1(neutral), similar to the $HOSO_2^-$ + HOCl reaction, the first step involves the barrierless transfer of Cl^+ from HOCl to the S atom of SO_3^{2-}, forming the $ClSO_3^-$ intermediate, plus a OH^- ion which likely leaves the reacting system due to electrostatic repulsion ($M_{6'}$). The lack of a barrier suggests that the rate of this reaction step is controlled by diffusion in the cloud water (see Eq (5)), and is therefore likely to be very rapid. Our calculations thus verify the efficient formation of the $ClSO_3^-$

intermediate which has not yet been characterized experimentally. $ClSO_3^-$ will subsequently react with H_2O to form sulfate through the hydrolysis reaction already presented in Fig. 3(a), with catalytic effects e.g. from another H_2O molecule as discussed above.

The HO^+ transfer mechanism (Pathway 2(neutral) in Fig. 5(b)) begins with the formation of a HOCl...SO_3^{2-} reactant complex (labelled R_{c7}), which then crosses a fairly low barrier (6.7 kcal/mol relative to the isolated reactant; labelled TS_7), leading directly to HSO_4^- and Cl^-. This low-barrier pathway, which was not considered in previous investigations, is likely the most competitive mechanism for sulfate formation in near-neutral conditions. (As discussed below, it is actually the dominant mechanism for all conditions.)

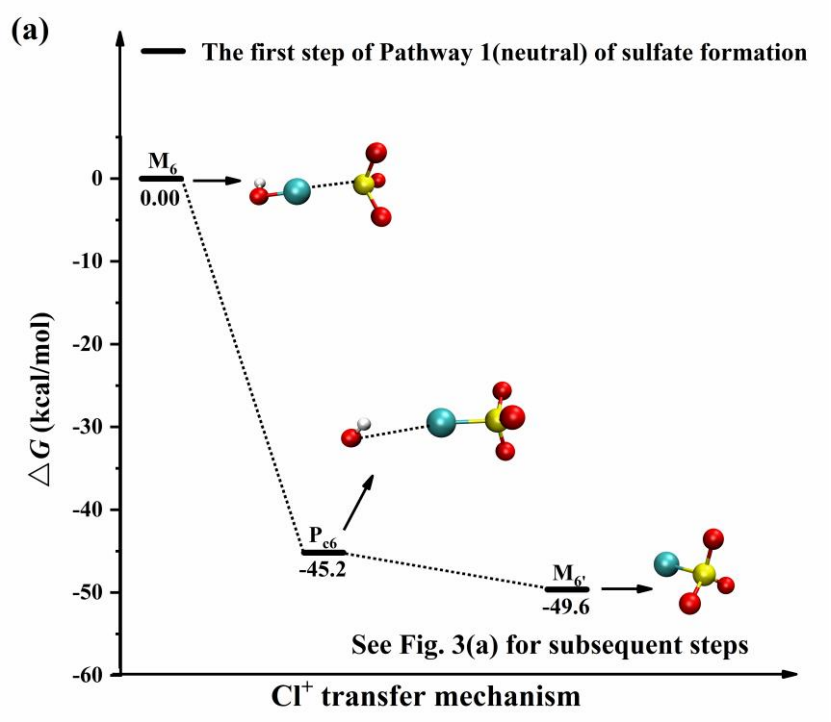

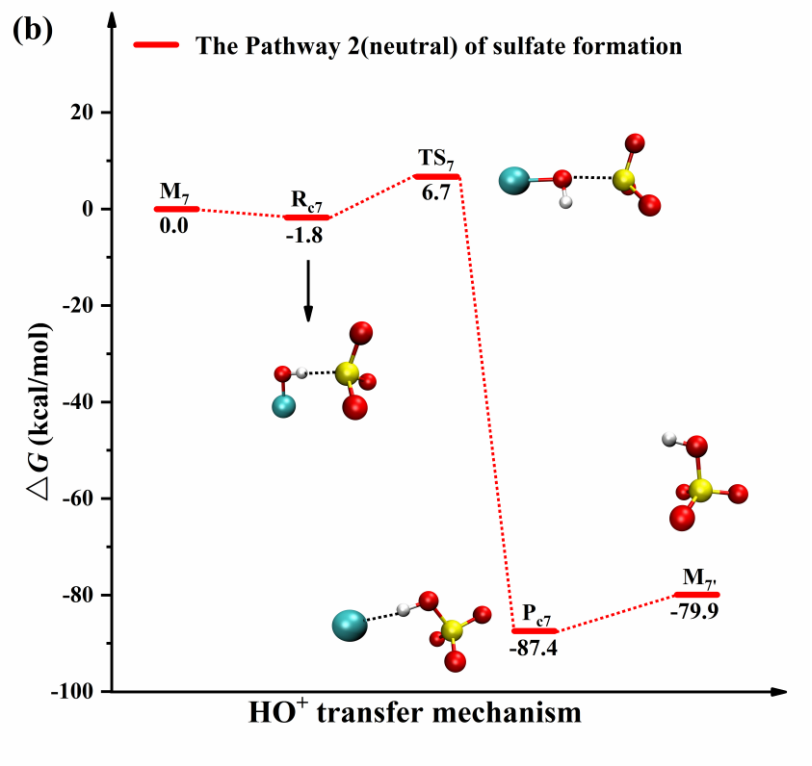

373

374 **Fig. 5.** The activation Gibbs free energy profile (kcal/mol, at 298.15 K and a reference concentration
375 of 1 mol/L) for the reaction of HOCl with SO_3^{2-} through the (a) Pathway 1(neutral) and the (b)
376 Pathway 2(neutral) at the CCSD(T)-F12/cc-pVDZ-F12//M06-2X/6-311++G (3df, 3pd) level of
377 theory. Solvent corrections are included in the M06-2X calculations using the SMD model. The
378 white, cyan, red, and yellow spheres represent H, Cl, O, and S atoms, respectively.

379 **3.3. Sulfate formation mechanism in alkaline water (7.5 ≤ pH ≤ 9.0)**

380 In the marine areas, when the cloud water is mixed with fresh sea-salt spray, the
381 atmospheric liquid phase may occasionally be alkaline rather than acidic. With the
382 increase of pH, the fraction of HOCl decreases, and OCl^- becomes to the dominant form
383 of hypochloric acid. Therefore, in the alkaline cloud water, the oxidation of S(IV) by
384 hypochloric acid could take place via a $OCl^- + SO_3^{2-}$ reaction. While hindered somewhat
385 by electrostatic repulsion (accounted for here using a modified version of the diffusion

rate coefficient, see Eq (7)), this anion-anion reaction has already been proposed to be feasible in experimental studies(Fogelman et al., 1989). In addition to the O atom transfer mechanism (Pathway 2(alkaline)) proposed in experimental studies(Fogelman et al., 1989), ESP results indicate that a Cl^+ transfer mechanism (Pathway 1(alkaline)) analogous to that found in weakly acidic or neutral conditions may also be possible in alkaline conditions. This mechanism is driven by the attraction between the chloride atom of OCl^- and the sulfur atom of SO_3^{2-}, as illustrated in the ESP analysis shown in Fig. 6. Here, the chlorine atom (site 6) of OCl^- possesses more positive ESP, giving it potential to react with the sulfur atom (site 4) of SO_3^{2-} with more negative ESP. We have thus investigated both O and Cl^+ transfer mechanisms also for alkaline conditions.

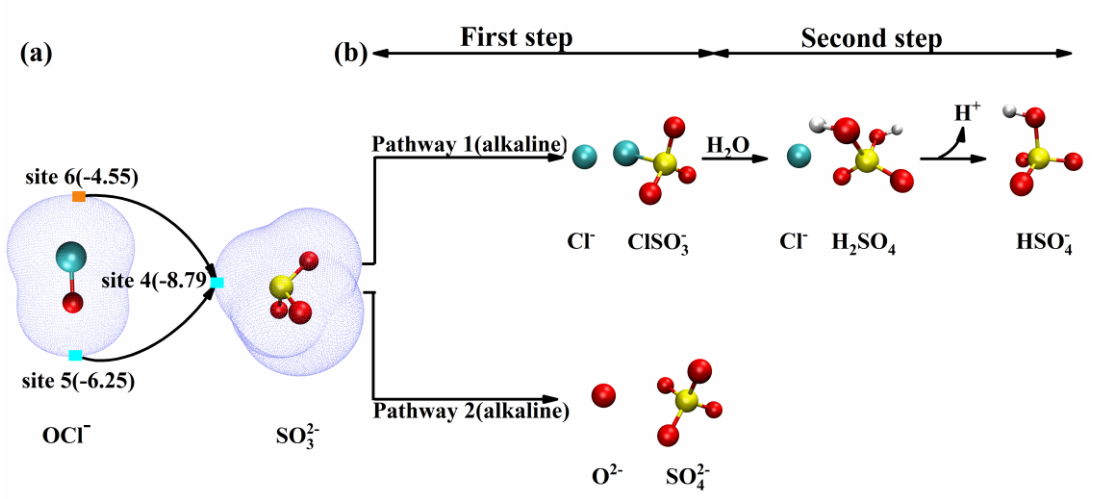

Fig. 6. (a) ESP-mapped molecular vdW surface of OCl^- and SO_3^{2-}, in units of kcal/mol. Surface local minima and maxima of ESPs of different functional groups in the corresponding molecules are represented as blue and orange squares, respectively. (b) Two possible reaction pathways for the reaction of SO_3^{2-} with OCl^- leading to sulfate formation. The cyan, red, and yellow spheres represent Cl, O, and S atoms, respectively.

The potential energy profiles and the corresponding geometries on the reaction path from OCl^- and SO_3^{2-} are shown in Figs. 7(a) and (b), respectively. Pathway 1(alkaline) begins with the formation of a $SO_3^{2-}\ldots OCl^-$ complex (R_{c8}). Despite the electrostatic repulsion between two anions, our solvent-corrected calculations predict that this complex is only 3.8 kcal/mol above the separated reactants in free energy. R_{c8} is connected to a linear transition state TS_8, leading to the formation of the $ClSO_3^-$ intermediate and O^{2-} ($M_{8'}$) with a free energy barrier of 14.0 kcal/mol. $ClSO_3^-$ then reacts with H_2O to form sulfate as shown in Fig. 3(a). Analogous to the acidic and neutral cases, Pathway 1(alkaline) can also be catalyzed by a H_2O molecule. The first step on this pathway is the formation of $SO_3^{2-}\ldots OCl^-\ldots H_2O$ complex (R_{c9}), which is connected to transition state TS_9. In TS_9, the Cl^+ of OCl^- interacts with the S atom of SO_3^{2-}, forming the $ClSO_3^-$ intermediate (which again hydrolyses as shown in Fig. 3(a)). Meanwhile, the O^{2-} leaving group of OCl^- accepts a proton from H_2O, producing two hydroxyls (OH^-) ions, much more stable products than the O^{2-} formed in the uncatalyzed mechanism. The free energy barrier for the catalyzed mechanism is accordingly 5.4 kcal/mol lower than that of the uncatalyzed mechanism. Although the formation of $ClSO_3^-$ intermediates in the Cl^+ transfer mechanism in alkaline conditions was not considered in previous studies(Fogelman et al., 1989), our calculations indicate that it is highly like to form on both the catalyzed and uncatalyzed reaction pathways.

Pathway 2(alkaline) of the $OCl^- + SO_3^{2-}$ reaction, shown in Fig. 7(b), also starts with the formation of a $SO_3^{2-}\ldots OCl^-$ complex (R_{c10}). R_{c10} differs from R_{c9} in the relative orientation of OCl^- with respect to SO_3^{2-}, as shown in Fig. 7(b). R_{c10} is connected to

transition state TS_{10}, with a free energy barrier of 20.3 kcal/mol relative to the isolated reactants, leading directly to the SO_4^{2-} and Cl^- product monomers (labelled $M_{10'}$). This pathway can also be catalyzed by H_2O. The catalyzed reaction starts with the formation of a $SO_3^{2-}\ldots OCl^-\ldots H_2O$ reactant complex (R_{c11}), which is converted into a $SO_4^{2-}\ldots Cl^-\ldots H_2O$ product complex (P_{c11}) via the transition state TS_{11}. The free energy barrier of this process (relative to the isolated reactants) is 2.0 kcal/mol lower than that of the uncatalyzed pathway. Analogous to Pathway 2(acidic), we thus predict a modest catalytic effect of water on Pathway 2(alkaline). The contour maps of the electron density difference between reactant complex R_{c11} and transition state TS_{11} (see Fig. S3) indicate that the oxygen atom of OCl^- transfers to the sulfur atom of SO_3^{2-}, forming a new O-S bond, while the remaining chloride ion is cleaved from the oxygen atom of OCl^-.

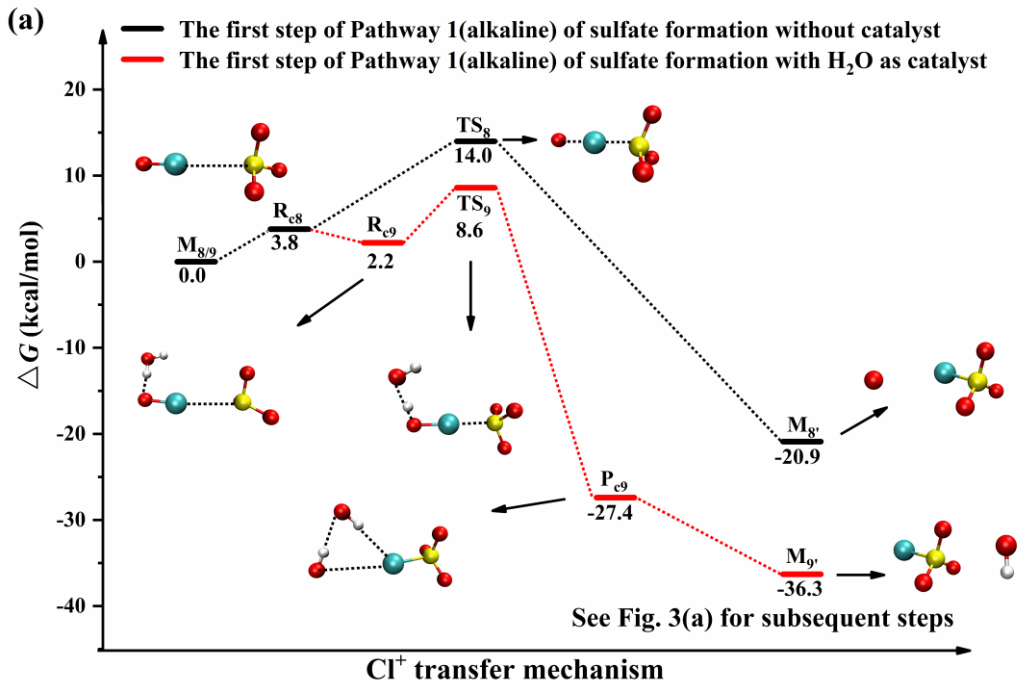

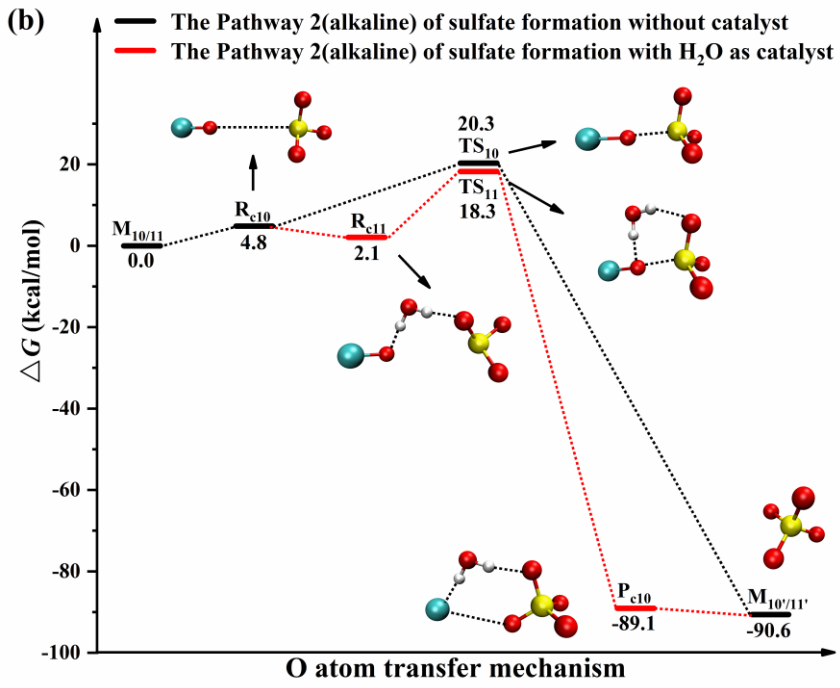

437

438 **Fig. 7.** The Gibbs free energy profile (kcal/mol, at 298.15 K and a reference concentration of 1

439 mol/L) for the reaction of OCl^- with SO_3^{2-} through (a) Pathway 1(alkaline) and (b) Pathway

440 2(alkaline), at the CCSD(T)-F12/cc-pVDZ-F12//M06-2X/6-311++G (3df, 3pd) level of theory.

441 Solvent corrections are included in the M06-2X calculations using the SMD model The white, cyan,

442 red, and yellow spheres represent H, Cl, O, and S atoms, respectively.

443 ## 4. Atmospheric Implication

444 Tables 1, 2 and 3 show the S(IV) oxidation rates, and corresponding lifetimes,

445 estimated for the six different pathways, applying the pseudo-steady-state

446 approximation to all intermediates, and using a constant aqueous-phase HOCl

447 concentration of 3.43×10^{-9}M. This concentration corresponds to an aqueous phase in

448 Henry's law equilibrium at 298.15 *K* with a gas phase containing 0.005 ppbv HOCl.

449 While this gas-phase mixing ratio represents the lower end of the experimentally

450 reported range (0.005 ppbv - 0.173ppbv), our assumption of a Henry's law equilibrium

451 correspondingly represents an upper-limit estimate, which likely does not hold
452 especially at higher pH as discussed below. We also note that while the pseudo-
453 unimolecular S(IV) oxidation rates and S(IV) lifetimes by definition do not depend on
454 the total S(IV) concentration, the rates and lifetimes of each individual channel still
455 depend on the fractional populations of the different S(IV) reactants ($HOSO_2^-$ and
456 SO_3^{2-}). As these are pH – dependent, also the rates and lifetimes vary with the pH. The
457 alkaline pathways have a further pH – dependence through the concentration of the
458 OCl^- reactant. For details of the rate and lifetime calculations, see the Supplementary
459 Information.

460 Table 1. Calculated S(IV) oxidation rates ($\nu_{1acid,\ cat\text{-}S(IV)}$ and $\nu_{2acid,\ cat\text{-}S(IV)}$) and S(IV)
461 lifetimes for Pathway 1(acidic) and Pathway 2(acidic) from $HOSO_2^-$ and HOCl with
462 H_2O as a catalyst, respectively, assuming [HOCl] =3.43×10^{-9} M (corresponding to a
463 Henry's law equilibrium with a gas phase HOCl mixing ratio of 0.005ppbv), and [H_2O]
464 =55.56 M (corresponding to the known bulk concentration of H_2O).

	Pathway 1(acidic)		Pathway 2(acidic)	
pH	$\nu_{1acid,\ cat\text{-}S(IV)}$ (s^{-1})	Lifetime (s)	$\nu_{2acid,\ cat\text{-}S(IV)}$ (s^{-1})	Lifetime (s)
3	5.25×10^{-17}	1.90×10^{16}	9.77×10^{-10}	1.02×10^{9}
4	5.55×10^{-17}	1.80×10^{16}	1.03×10^{-9}	9.68×10^{8}
5	5.53×10^{-17}	1.81×10^{16}	1.03×10^{-9}	9.72×10^{8}
6	5.05×10^{-17}	1.98×10^{16}	9.40×10^{-10}	1.06×10^{9}
6.5	4.18×10^{-17}	2.39×10^{16}	7.77×10^{-10}	1.29×10^{9}

7	2.70×10^{-17}	3.70×10^{16}	5.02×10^{-10}	1.99×10^{9}
7.5	1.27×10^{-17}	7.85×10^{16}	2.37×10^{-10}	4.22×10^{9}
8	4.77×10^{-18}	2.10×10^{17}	8.88×10^{-11}	1.13×10^{10}
9	5.17×10^{-19}	1.93×10^{18}	9.62×10^{-12}	1.04×10^{11}

Table 2. The calculated S(IV) oxidation rates ($\nu_{1neu,\ cat\text{-}S(IV)}$ and $\nu_{2neu\text{-}S(IV)}$) and the S(IV) lifetimes for Pathway 1(neutral) (with H_2O as a catalyst) and Pathway 2(neutral) from SO_3^{2-} and HOCl, respectively, assuming [HOCl] $=3.43\times10^{-9}$ M (corresponding to a Henry's law equilibrium with a gas phase HOCl mixing ratio of 0.005ppbv), and [H_2O] =55.56 M (corresponding to the known bulk concentration of H_2O).

	Pathway 1(neutral)		Pathway 2(neutral)	
pH	$\nu_{1neu,\ cat\text{-}S(IV)}$ (s^{-1})	Lifetime (s)	$\nu_{2neu\text{-}S(IV)}$ (s^{-1})	Lifetime (s)
3	5.79×10^{-20}	1.73×10^{19}	2.59×10^{-5}	3.87×10^{4}
4	6.12×10^{-19}	1.63×10^{18}	2.73×10^{-4}	3.66×10^{3}
5	6.09×10^{-18}	1.64×10^{17}	2.72×10^{-3}	3.67×10^{2}
6	5.57×10^{-17}	1.80×10^{16}	2.49×10^{-2}	4.02×10^{1}
6.5	1.46×10^{-16}	6.87×10^{15}	6.51×10^{-2}	1.54×10^{1}
7	2.98×10^{-16}	3.36×10^{15}	1.33×10^{-1}	7.52
7.5	4.44×10^{-16}	2.25×10^{15}	1.98×10^{-1}	5.04
8	5.26×10^{-16}	1.90×10^{15}	2.35×10^{-1}	4.25
9	5.70×10^{-16}	1.75×10^{15}	2.55×10^{-1}	3.93

Table 3. The calculated S(IV) oxidation rates ($v_{1alk,\ cat\text{-}S(IV)}$ and $v_{2alk,\ cat\text{-}S(IV)}$) and S(IV) lifetimes for Pathway 1(alkaline) and Pathway 2(alkaline) from SO_3^{2-} and OCl^- with H_2O as a catalyst, respectively, assuming [HOCl] =3.43×10^{-9} M (corresponding to a Henry's law equilibrium with a gas phase HOCl mixing ratio of 0.005ppbv), and [H_2O] =55.56 M (corresponding to the known bulk concentration of H_2O).

	Pathway 1(neutral)		Pathway 2(neutral)	
pH	$v_{1alk,\ cat\text{-}S(IV)}$ (s^{-1})	Lifetime (s)	$v_{2alk,\ cat\text{-}S(IV)}$ (s^{-1})	Lifetime (s)
3	1.71×10^{-26}	5.85×10^{25}	1.43×10^{-16}	7.00×10^{15}
4	1.81×10^{-24}	5.53×10^{23}	1.51×10^{-14}	6.63×10^{13}
5	1.80×10^{-22}	5.56×10^{21}	1.50×10^{-12}	6.65×10^{11}
6	1.64×10^{-20}	6.08×10^{19}	1.37×10^{-10}	7.28×10^{9}
6.5	1.36×10^{-19}	7.35×10^{18}	1.14×10^{-9}	8.80×10^{8}
7	8.79×10^{-19}	1.14×10^{18}	7.34×10^{-9}	1.36×10^{8}
7.5	4.15×10^{-18}	2.41×10^{17}	3.47×10^{-8}	2.89×10^{7}
8	1.55×10^{-17}	6.44×10^{16}	1.30×10^{-7}	7.70×10^{6}
9	1.68×10^{-16}	5.94×10^{15}	1.41×10^{-6}	7.11×10^{5}

Our results indicate that the HO^+ transfer mechanism (Pathway 2(neutral)) from SO_3^{2-} + HOCl completely dominates sulfate formation through the HOCl + S(IV) reaction at all atmospherically relevant pH, despite the relatively low fractional populations of SO_3^{2-} at low pH and HOCl at high pH. Even at a pH of 9, the second-fastest reaction mechanism (Pathway 2(alkaline)) is still over five orders of magnitude

slower than Pathway 2(neutral).

The explanation for this is simple: Pathway 2(neutral) has a much lower rate-limiting barrier than any of the other channels, leading to an essentially diffusion-limited rate constant. Pathways 1(acidic), 1(neutral) and 1(alkaline) all involve a $ClSO_3^-$ hydrolysis step, which has a substantial barrier even after catalysis by a third body such as H_2O (see Fig. 3(a)). Pathways 2(acidic) and 2(alkaline) have lower but still substantial barriers, which are only modestly lowered by catalysts. The rates of both alkaline pathways are further decreased by electrostatic repulsion between the reactant anions.

Our simple lifetime estimates show that if HOCl is present in the aqueous phase, the HOCl + S(IV) reaction is likely to be competitive with other known S(IV) oxidation channels for the full studied pH range of 3 to 9. Especially toward the upper end of this range, the computed lifetimes are unrealistically short, as experimentally measured lifetimes for liquid-phase S(IV) are seldom below about 1000 s(Berglen, 2004; Fang et al., 2019; Kasting et al., 1987; Lelieveld and Heintzenberg, 1992; Wang et al., 2020; Zhang et al., 2020). The explanation for this discrepancy is that especially at higher pH, depletion of HOCl through the HO^+ transfer from SO_3^{2-} + HOCl reaction (Pathway 2(neutral)) is so rapid that the Henry's law equilibrium between the gas phase and the aqueous phase will never have time to form. S(IV) oxidation will then be controlled by the rate of diffusion and dissolution of gas-phase HOCl to the liquid phase. We also note that the rapid depletion of HOCl through the direct HO^+ transfer reaction may also help explain the absence of experimental observations of $ClSO_3^-$ or other intermediates,

503 despite the fact that their formation is also predicted to be rapid.

504 The extremely rapid S(IV) oxidation by HOCl predicted by our calculations may
505 help explain observations of unexpectedly efficient sulfate formation in marine areas.
506 While S(IV) + HOCl reactions have been proposed previously(Fogelman et al., 1989;
507 Liu and Abbatt, 2020), our results reveal that the dominant reaction mechanism is
508 different from previous speculations. Chemistry-transport modelling incorporating the
509 pH-dependent reaction mechanism proposed here, and accounting for the rate-limiting
510 gas-liquid mass transfer of HOCl, will likely be useful for improving regional and
511 global sulfate budgets. Finally, hypobromic acid (HOBr) is chemically very similar to
512 hypochloric acid, and might conceivably also contribute to S(IV) oxidation and thus
513 sulfate formation in marine areas. The S(IV) + HOBr reaction should therefore be
514 explored in the future.

515 ## 5. Conclusion

516 We have performed high-level quantum chemical calculations to comprehensively
517 examine the mechanism for sulfate formation through the oxidation of dissolved
518 sulfurous acid (denoted S(IV)) by hypochloric acid over wide range of pH (from 3.0 to
519 9.0). Our results demonstrate that while previously proposed Cl^+ transfer mechanisms
520 exist, and might be catalyzed by e.g. H_2O molecules, sulfate formation from the S(IV)
521 + HOCl reaction is completely dominated by a novel low-barrier HO^+ transfer
522 mechanism from HOCl + SO_3^{2-}. This reaction mechanism forms sulfate directly,
523 without involving intermediates such as $ClSO_3^-$, which likely explains the puzzling lack
524 of observations of such intermediates in experimental studies. The rate of S(IV)

oxidation via this reaction increases with pH due to the increasing fractional population of SO_3^{2-}. Even in acidic conditions (pH = 3), the S(IV) lifetime predicted for this reaction, assuming a liquid phase in Henry's law equilibrium with a gas-phase containing 5 pptv HOCl, is less than nine hours. At higher pH, the rate of HOCl depletion is likely so rapid that the Henry's law equilibrium will not hold, and S(IV) oxidation will be controlled by mass transfer of HOCl to the liquid phase. The HOCl + SO_3^{2-} reaction mechanism proposed here is likely to help explain sulfate formation missing from current atmospheric chemistry models, and thus narrow the gap between field observations and modelling on the distribution of sulfate, as well as improve our overall understanding of marine secondary aerosol.

Declaration of competing interest

The authors declare that they have no known competing financial interests or personal relationships that could have appeared to influence the work reported in this paper.

Acknowledgements

We thank the National Natural Science Foundation of China (21976015). L. L. thanks the China Postdoctoral Science Foundation (Grant 2020M680013). T. K. thanks the Academy of Finland for Funding and the CSC – IT Center for Science for computer resources.

CRediT authorship contribution statement

Jiarong Liu: Data curation, Formal analysis, Investigation, Writing - original draft; Writing - review & editing. An Ning and Ling Liu: Supervision; Validation,

Visualization. Huixian Wang: Supervision; Validation. Theo Kurtén: Writing - review & editing, Methodology, Formal analysis. Xiuhui Zhang: Conceptualization, Writing - review & editing, Formal analysis, Data curation.

6. References:

Alexander, B., Park, R. J., Jacob, D. J., Gong, S., 2009. Transition metal-catalyzed oxidation of atmospheric sulfur: Global implications for the sulfur budget. J. Geophys. Res., 114, D2309, http://doi.org/10.1029/2008JD010486

Alexander, B., Allman, D. J., Amos, H. M., Fairlie, T. D., Dachs, J., Hegg, D. A., Sletten, R. S., 2012. Isotopic constraints on the formation pathways of sulfate aerosol in the marine boundary layer of the subtropical northeast Atlantic Ocean. J. Geophys. Res., 117, D6304, http://doi.org/10.1029/2011JD016773

Almeida, J., Schobesberger, S., Kurten, A., Ortega, I. K., Kupiainen-Maatta, O., Praplan, A. P., Adamov, A., Amorim, A., Bianchi, F., Breitenlechner, M., David, A., Dommen, J., Donahue, N. M., Downard, A., Dunne, E., Duplissy, J., Ehrhart, S., Flagan, R. C., Franchin, A., Guida, R., Hakala, J., Hansel, A., Heinritzi, M., Henschel, H., Jokinen, T., Junninen, H., Kajos, M., Kangasluoma, J., Keskinen, H., Kupc, A., Kurten, T., Kvashin, A. N., Laaksonen, A., Lehtipalo, K., Leiminger, M., Leppa, J., Loukonen, V., Makhmutov, V., Mathot, S., McGrath, M. J., Nieminen, T., Olenius, T., Onnela, A., Petaja, T., Riccobono, F., Riipinen, I., Rissanen, M., Rondo, L., Ruuskanen, T., Santos, F. D., Sarnela, N., Schallhart, S., Schnitzhofer, R., Seinfeld, J. H., Simon, M., Sipila, M., Stozhkov, Y., Stratmann, F., Tome, A., Trostl, J., Tsagkogeorgas, G., Vaattovaara, P., Viisanen, Y., Virtanen, A., Vrtala, A., Wagner, P. E., Weingartner, E., Wex, H., Williamson, C., Wimmer, D., Ye, P., Yli-Juuti, T., Carslaw, K. S., Kulmala, M., Curtius, J., Baltensperger, U., Worsnop, D. R., Vehkamaki, H., Kirkby, J., 2013. Molecular understanding of sulphuric acid-amine particle nucleation in the atmosphere. Nature, 502, 359-363, http://doi.org/10.1038/nature12663

Baird, N. C., Taylor, K. F., 1981. Ab initio MO calculations for the oxides, oxyacids, and oxyanions of S(IV)and S(VI). J. Comput. Chem., 2, 225-230, http://doi.org/10.1002/jcc.540020303

Berglen, T. F., 2004. A global model of the coupled sulfur/oxidant chemistry in the troposphere: The sulfur cycle. J. Geophys. Res., 109, D19310, http://doi.org/10.1029/2003JD003948

Brandt, C., van Eldik, R., 1995. Transition metal-catalyzed oxidation of sulfur (IV) oxides. Atmospheric-relevant processes and mechanisms. Chem. Rev, 95, 119-190, http://doi.org/10.1021/cr00033a006

Brown, R. E., Barber, F., 1995. Ab initio studies of the thermochemistry of the bisulfite and the sulfonate ions and

related compounds. J. Phys. Chem., 99, 8071-8075, http://doi.org/10.1021/j100020a034

C. Drexler, H. E., Fecher, B., Wannowius, K. J., 1992. Kinetics and mechanism of sulfur (IV) oxidation by hydrogen peroxide in aqueous phase: the non-linear parts of the pH-profile. Bur. Bunsenges. Phys., 96, 481-485, http://doi.org/10.1002/bbpc.19920960349

Chandler, A. S., Choularton, T. W., Dollardt, G. J., Eggleton, A. E. J., Gay, M. J., Hill, T. A., Jones, B. M. R., Tyler, B. J., Bandy, B. J., Penkett, S. A., 1988. Measurements of H_2O_2 and SO_2 in clouds and estimates of their reaction rate. Nature, 336, 562-565, http://doi.org/10.1038/336562a0

Chang, R., 2000. Physical Chemistry for the Chemical and Biological Sciences. Sausalito, CA.

Chen, J., Shao, Y., Ho, J., 2019. Are explicit solvent models more accurate than implicit solvent models? a case study on the menschutkin reaction. J. Phys. Chem. A, 123, 5580-5589, http://doi.org/10.1021/acs.jpca.9b03995

Chen, Q., Sherwen, T., Evans, M., Alexander, B., 2018. DMS oxidation and sulfur aerosol formation in the marine troposphere: a focus on reactive halogen and multiphase chemistry. Atmos. Chem. Phys., 18, 13617-13637, http://doi.org/10.5194/acp-2018-410

Chen, Q., Geng, L., Schmidt, J. A., Xie, Z., Kang, H., Dachs, J., Cole-Dai, J., Schauer, A. J., Camp, M. G., Alexander, B., 2016. Isotopic constraints on the role of hypohalous acids in sulfate aerosolformation in the remote marine boundary layer. Atmos. Chem. Phys., 16, 11433-11450, http://doi.org/10.5194/acp-16-11433-2016

Chen, Q., Schmidt, J. A., Shah, V., Jaeglé, L., Sherwen, T., Alexander, B., 2017. Sulfate production by reactive bromine: Implications for the global sulfur and reactive bromine budgets. Geophys. Res. Lett., 44, 7069-7078, http://doi.org/10.1002/2017GL073812

Cheng, Y., Zheng, G., Wei, C., Mu, Q., Zheng, B., Wang, Z., Gao, M., Zhang, Q., He, K., Carmichael, G., Poschl, U., Su, H., 2016. Reactive nitrogen chemistry in aerosol water as a source of sulfate during haze events in China. Sci Adv, 2, e1601530, http://doi.org/10.1126/sciadv.1601530

Choi, Y., Rhee, T. S., Collett, J. L., Park, T., Park, S., Seo, B., Park, G., Park, K., Lee, T., 2017. Aerosol concentrations and composition in the North Pacific marine boundary layer. Atmos. Environ., 171, 165-172, http://doi.org/10.1016/j.atmosenv.2017.09.047

Clifton, C. L., Altstein, N., Huie, R. E., 1988. Rate constant for the reaction of nitrogen dioxide with sulfur (IV) over the pH range 5.3-13. Environ. Sci. Technol., 22, 586-589, http://doi.org/10.1021/es00170a018

Collins, F. C., Kimball, G. E., 1949. Diffusion-controlled reaction rates. J. Colloid Interf. Sci., 4, 425-437, http://doi.org/10.1016/0095-8522(49)90023-9

Dowd, C. D. O., Facchini, M. C., Cavalli, F., Ceburnis, D., Mircea, M., Decesari, S., Fuzzi, S., Yoon, Y. J., Putaud,

J., 2004. Biogenically driven organic contribution to marine aerosol. Nature, 431, 676-680, http://doi.org/10.1038/nature02959

Dumka, U. C., Ningombam, S. S., Kaskaoutis, D. G., Madhavan, B. L., Song, H. J., Angchuk, D., Jorphail, S., 2020. Long-term (2008–2018) aerosol properties and radiative effect at high-altitude sites over western trans-Himalayas. Sci. Total Environ., 734, 139354, http://doi.org/10.1016/j.scitotenv.2020.139354

Ehn, M., Thornton, J. A., Kleist, E., Sipilä, M., Junninen, H., Pullinen, I., Springer, M., Rubach, F., Tillmann, R., Lee, B., Lopez-Hilfiker, F., Andres, S., Acir, I., Rissanen, M., Jokinen, T., Schobesberger, S., Kangasluoma, J., Kontkanen, J., Nieminen, T., Kurtén, T., Nielsen, L. B., Jørgensen, S., Kjaergaard, H. G., Canagaratna, M., Maso, M. D., Berndt, T., Petäjä, T., Wahner, A., Kerminen, V., Kulmala, M., Worsnop, D. R., Wildt, J., Mentel, T. F., 2014. A large source of low-volatility secondary organic aerosol. Nature, 506, 476-479, http://doi.org/10.1038/nature13032

Einstein, A., 1905. On the movement of small particles suspended in stationary liquids required by the molecular-kinetic theory of heat. Ann. Phys., 17, 549-560,

Elm, J., Bilde, M., Mikkelsen, K. V., 2012. Assessment of density functional theory in predicting structures and free energies of reaction of atmospheric prenucleation clusters. J. Chem. Theory Comput., 8, 2071-2077, http://doi.org/10.1021/ct300192p

Evans, M. G., Polanyi, M., 1935. Some applications of the transition state method to the calculation of reaction velocities, especially in solution. Trans. Faraday Soc., 31, 875-893, http://doi.org/10.1039/TF9353100875

Eyring, H., 1935. The activated complex in chemical reactions. J. Chem. Phys., 3, 107-115, http://doi.org/10.1063/1.1749604

Fang, Y., Ye, C., Wang, J., Wu, Y., Hu, M., Lin, W., Xu, F., Zhu, T., 2019. Relative humidity and O_3 concentration as two prerequisites for sulfate formation. Atmos. Chem. Phys., 19, 12295-12307, http://doi.org/10.5194/acp-19-12295-2019

Fogelman, K. D., Walker, D. M., Margerum, D. W., 1989. Non-metal redox kinetics: hypochlorite and hypochlorous acid reactions with sulfite. Inorg. Chem., 28, 986-993, http://doi.org/10.1002/chin.198925018

Fridlind, A. M., Jacobson, M. Z., 2000. A study of gas-aerosol equilibrium and aerosol pH in the remote marine boundary layer during the First Aerosol Characterization Experiment (ACE 1). J. Geophys. Res. Atmos., 105, 17325-17340, http://doi.org/10.1029/2000JD900209

Frisch, M. J., Trucks, G. W., Schlegel, H. B., Scuseria, G. E., Robb, M. A., Cheeseman, J. R., Scalmani, G., Barone, V., Petersson, G. A., Nakatsuji, H., Li, X., Caricato, M., Marenich, A. V., Bloino, J., Janesko, B. G., Gomperts,

R., Mennucci, B., Hratchian, H. P., Ortiz, J. V., Izmaylov, A. F., Sonnenberg, J. L., Williams-Young, D., Ding, F., Lipparini, F., Egidi, F., Goings, J., Peng, B., Petrone, A., Henderson, T., Ranasinghe, D., Zakrzewski, V. G., Gao, J., Rega, N., Zheng, G., Liang, W., Hada, M., Ehara, M., Toyota, K., Fukuda, R., Hasegawa, J., Ishida, M., Nakajima, T., Honda, Y., Kitao, O., Nakai, H., Vreven, T., Throssell, K., Montgomery, J. A., Peralta, J. E., Ogliaro, F., Bearpark, M. J., Heyd, J. J., Brothers, E. N., Kudin, K. N., Staroverov, V. N., Keith, T. A., Kobayashi, R., Normand, J., Raghavachari, K., Rendell, A. P., Burant, J. C., Iyengar, S. S., Tomasi, J., Cossi, M., Millam, J. M., Klene, M., Adamo, C., Cammi, R., Ochterski, J. W., Martin, R. L., Morokuma, K., Farkas, O., Foresman, J. B., Fox, D. J., 2016. Gaussian, Inc., Wallingford CT. Gaussian, Inc., Wallingford CT,

Gen, M., Zhang, R., Huang, D. D., Li, Y., Chan, C. K., 2019. Heterogeneous SO_2 oxidation in sulfate formation by photolysis of particulate nitrate. Environ. Sci. Technol. Lett., 6, 86-91, http://doi.org/10.1021/acs.estlett.8b00681

Harris, E., Sinha, B., van Pinxteren, D., Tilgner, A., Fomba, K. W., Schneider, J., Roth, A., Gnauk, T., Fahlbusch, B., Mertes, S., Lee, T., Collett, J., Foley, S., Borrmann, S., Hoppe, P., Herrmann, H., 2013. Enhanced role of transition metal ion catalysis during in-cloud oxidation of SO_2. Science, 340, 727-730, http://doi.org/10.1126/science.1230911

He, H., Wang, Y., Ma, Q., Ma, J., Chu, B., Ji, D., Tang, G., Liu, C., Zhang, H., Hao, J., 2014. Mineral dust and NO_x promote the conversion of SO_2 to sulfate in heavy pollution days. Sci Rep, 4, 1-5, http://doi.org/10.1038/srep04172

Horner, D. A., Connick, R. E., 1986. Equilibrium quotient for the isomerization of bisulfite ion from HSO_3^- to SO_3H^-. Inorg. Chem, 25, 2414-2417, http://doi.org/10.1021/ic00234a026

Huang, S., Wu, Z., Poulain, L., van Pinxteren, M., Merkel, M., Assmann, D., Herrmann, H., Wiedensohler, A., 2018. Source apportionment of the submicron organic aerosols over the Atlantic Ocean from 53°N to 53°S using HR-ToF-AMS. Atmos. Chem. Phys, 24, 18043-18062, http://doi.org/10.5194/acp-2018-307

Huang, X., Song, Y., Zhao, C., Li, M., Zhu, T., Zhang, Q., Zhang, X., 2014. Pathways of sulfate enhancement by natural and anthropogenic mineral aerosols in China. J. Geophys. Res. Atmos., 119, 14165-14179, http://doi.org/10.1002/2014JD022301

Humphrey, W., Dalke, A., Schulten, K., 1996. VMD: Visual molecular dynamics. J Mol Graph, 14, 33-38, http://doi.org/https://doi.org/10.1016/0263-7855(96)00018-5

Hung, H., Hsu, M., Hoffmann, M. R., 2018. Quantification of SO_2 oxidation on interfacial surfaces of acidic micro-droplets: Implication for ambient sulfate formation. Environ. Sci. Technol., 52, 9079-9086,

http://doi.org/10.1021/acs.est.8b01391

Hung, H., Hoffmann, M. R., 2015. Oxidation of gas-phase SO_2 on the surfaces of acidic microdroplets: implications for sulfate and sulfate radical anion formation in the atmospheric liquid phase. Environ. Sci. Technol., 49, 13768-13776, http://doi.org/10.1021/acs.est.5b01658

Kasting, J. F., Liu, M. S., Toon, O. B., Turco, R. P., 1987. The sulfur cycle in the marine atmosphere. J. Geophys. Res. Atmos., 92, 943-963, http://doi.org/10.1029/JD092iD01p00943

Keene, W. C., Sander, R., Pszenny, A. A. P., Vogt, R., Crutzen, P. J., Galloway, J. N., 1998. Aerosol pH in the marine boundary layer: A review and model evaluation. J. Aerosol Sci., 29, 339-356, http://doi.org/10.1016/S0021-8502(97)10011-8

Keshavarz, F., Thornton, J. A., Vehkamäki, H., Kurtén, T., 2021. Reaction mechanisms underlying unfunctionalized alkyl nitrate hydrolysis in aqueous aerosols. ACS Earth Space Chem., 5, 210-225, http://doi.org/10.1021/acsearthspacechem.0c00253

Kunen, S. M., Lazrus, A. L., Kok, G. L., Heike, B. G., 1983. Aqueous oxidation of SO_2: by hydrogen peroxid. J Geophys Res, 88, 3671-3674, http://doi.org/10.1029/JC088iC06p03671

Landim, A. A., Teixeira, E. C., Agudelo-Castañeda, D., Schneider, I., Silva, L. F. O., Wiegand, F., Kumar, P., 2018. Spatio-temporal variations of sulfur dioxide concentrations in industrial and urban area via a new statistical approach. Air Qual Atmos Health, 11, 801-813, http://doi.org/10.1007/s11869-018-0584-2

Lane, J. R., Kjaergaard, H. G., 2009. Explicitly correlated intermolecular distances and interaction energies of hydrogen bonded complexes. J. Chem. Phys., 131, 34307, http://doi.org/10.1063/1.3159672

Lelieveld, J., Heintzenberg, J., 1992. Sulfate cooling effect on climate through in-cloud oxidation of anthropogenic SO_2. Science, 258, 117-120, http://doi.org/10.1126/science.258.5079.117

Li, G., Bei, N., Cao, J., Huang, R., Wu, J., Feng, T., Wang, Y., Liu, S., Zhang, Q., Tie, X., Molina, L. T., 2017. A possible pathway for rapid growth of sulfate during haze days in China. Atmos. Chem. Phys., 17, 1-43, http://doi.org/10.5194/acp-2016-994

Li, H., Zhong, J., Vehkamäki, H., Kurtén, T., Wang, W., Ge, M., Zhang, S., Li, Z., Zhang, X., Francisco, J. S., Zeng, X. C., 2018. Self-catalytic reaction of SO_3 and NH_3 to produce sulfamic acid and its implication to atmospheric particle formation. J. Am. Chem. Soc., 140, 11020-11028, http://doi.org/10.1021/jacs.8b04928

Li, J., Han, Z., Yao, X., Xie, Z., Tan, S., 2019. The distributions and direct radiative effects of marine aerosols over East Asia in springtime. Sci. Total Environ., 651, 1913-1925, http://doi.org/10.1016/j.scitotenv.2018.09.368

Li, L., Hoffmann, M. R., Colussi, A. J., 2018. Role of nitrogen dioxide in the production of sulfate during Chinese

haze-aerosol episodes. Environ. Sci. Technol., 52, 2686-2693, http://doi.org/10.1021/acs.est.7b05222

Li, W., McKee, M. L., 1997. Theoretical study of OH and H_2O addition to SO_2. J. Phys. Chem. A, 101, 9778-9782, http://doi.org/10.1021/jp972389r

Liu, J., Fang, S., Wang, Z., Yi, W., Tao, F., Liu, J., 2015. Hydrolysis of sulfur dioxide in small clusters of sulfuric acid: mechanistic and kinetic study. Environ. Sci. Technol., 49, 13112-13120, http://doi.org/10.1021/acs.est.5b02977

Liu, T., Abbatt, J. P. D., 2020. An experimental assessment of the importance of S(IV) oxidation by hypohalous acids in the marine atmosphere. Geophys. Res. Lett., 47, 1-8, http://doi.org/10.1029/2019GL086465

Lu, T., Chen, F., 2012. Multiwfn: a multifunctional wavefunction analyzer. J. Comput. Chem., 33, 580-592, http://doi.org/10.1002/jcc.22885

Manzetti, S., Lu, T., 2013. The geometry and electronic structure of aristolochic acid: possible implications for a frozen resonance. J. Phys. Org. Chem., 26, 473-483, http://doi.org/10.1002/poc.3111

Mardirossian, N., Head-Gordon, M., 2016. How accurate are the minnesota density functionals for noncovalent interactions, isomerization energies, thermochemistry, and barrier heights involving molecules composed of main-group elements? J. Chem. Theory Comput., 12, 4303-4325, http://doi.org/10.1021/acs.jctc.6b00637

Marenich, A. V., Cramer, C. J., Truhlar, D. G., 2009. Performance of SM6, SM8, and SMD on the SAMPL 1 test set for the prediction of small-molecule solvation free energies. J. Phys. Chem. B, 113, 4538-4543, http://doi.org/10.1021/jp809094y

McArdle, J. V., Hoffmann, M. R., 1983. Kinetics and mechanism of the oxidation of aquated sulfur dioxide by hydrogen peroxide at low pH. J. Phys. Chem., 87, 5425-5429, http://doi.org/10.1021/j150644a024

Meijer, E. J., Sprik, M., 1998. A density functional study of the addition of water to SO_3 in the gas phase and in aqueous solution. J. Phys. Chem. A, 102, 2893-2898, http://doi.org/10.1021/jp972146z

Miguel, E. L. M., Santos, C. I. L., Silva, C. M., Jr. Pliego, J. R., 2016. How accurate is the SMD model for predicting free energy barriers for nucleophilic substitution reactions in polar protic and dipolar aprotic solvents? J. Braz. Chem. Soc., 27, 2055-2061, http://doi.org/10.5935/0103-5053.20160095

Minakata, D., Song, W., Mezyk, S. P., Cooper, W. J., 2015. Experimental and theoretical studies on aqueous-phase reactivity of hydroxyl radicals with multiple carboxylated and hydroxylated benzene compounds. Phys. Chem. Chem. Phys., 17, 11796-11812, http://doi.org/10.1039/c5cp00861a

Murray, J. S., Politzer, P., 2011. The electrostatic potential: an overview. Wires. Comput. Mol. Sci., 1, 153-163, http://doi.org/10.1002/wcms.19

Neese, F., 2012. The ORCA program system. Wires. Comput. Mol. Sci., 2, 73-78, http://doi.org/10.1002/wcms.81

Novakov, T., Rivera-Carpio, C., Penner, J. E., Rogers, C. F., 1994. The effect of anthropogenic sulfate aerosols on marine cloud droplet concentrations. Tellus, 46, 132-141, http://doi.org/10.1034/j.1600-0889.1994.t01-1-00005.x

O'Dowd, C. D., de Leeuw, G., 2007. Marine aerosol production: a review of the current knowledge. Phil. Trans. R. Soc. A., 365, 1753-1774, http://doi.org/10.1098/rsta.2007.2043

Ostovari, H., Zahedi, E., Sarvi, I., Shiroudi, A., 2018. Kinetic and mechanistic insight into the formation of amphetamine using the Leuckart–Wallach reaction and interaction of the drug with GpCCpG base-pair step of DNA: a DFT study. Monatshefte für Chemie - Chemical Monthly, 149, 1045-1057, http://doi.org/10.1007/s00706-018-2145-7

Peterson, K. A., Adler, T. B., Werner, H., 2008. Systematically convergent basis sets for explicitly correlated wavefunctions: The atoms H, He, B–Ne, and Al–Ar. J. Chem. Phys., 128, 84102, http://doi.org/10.1063/1.2831537

Pszenny, A. A. P., Moldanová, J., Keene, W. C., Sander, R., Maben, J. R., Martinez, M., Crutzen, P. J., Perner, D., Prinn, R. G., 2003. Halogen cycling and aerosol pH in the Hawaiian marine boundary layer. Atmos. Chem. Phys., 3, 4701-4753, http://doi.org/10.5194/acpd-3-4701-2003

Rong, H., Liu, L., Liu, J., Zhang, X., 2020. Glyoxylic sulfuric anhydride from the gas-phase reaction between glyoxylic acid and SO_3: A potential nucleation precursor. J. Phys. Chem. A, 124, 3261-3268, http://doi.org/10.1021/acs.jpca.0c01558

Roussel, M. R., 1985. Diffusion-influenced reactions. University of Lethbridge.

Shaka, H., Robertson, W. H., Finlayson-Pitts, B. J., 2007. A new approach to studying aqueous reactions using diffuse reflectance infrared Fourier transform spectrometry: application to the uptake and oxidation of SO_2 on OH-processed model sea salt aerosol. Phys. Chem. Chem. Phys., 9, 1980-1990, http://doi.org/10.1039/b612624c

Shen, X., Lee, T., Guo, J., Wang, X., Li, P., Xu, P., Wang, Y., Ren, Y., Wang, W., Wang, T., Li, Y., Carn, S. A., Collett, J. L., 2012. Aqueous phase sulfate production in clouds in eastern China. Atmos. Environ., 62, 502-511, http://doi.org/10.1016/j.atmosenv.2012.07.079

Smoluchowski, M. V., 1917. Mathematical Theory of the kinetics of the coagulation of colloidal solutions. Z. Phys. Chem., 92, 129-168,

Stokes, G. G., 1903. Mathematical and physical papers. U.K. Cambridge University Press.

Torrent-Sucarrat, M., Francisco, J. S., Anglada, J. M., 2012. Sulfuric acid as autocatalyst in the formation of sulfuric acid. J. Am. Chem. Soc., 134, 20632-20644, http://doi.org/10.1021/ja307523b

Truhlar, D. G., Hase, W. L., Hynes, J. T., 1983. Current status of transition-state theory. J. Phys. Chem., 87, 2664-2682, http://doi.org/10.1021/j100238a003

Truhlar, D. G., 1985. Nearly encounter-controlled reactions: The equivalence of the steady-state and diffusional viewpoints. J. Chem. Educ., 104-106, http://doi.org/10.1021/ed062p104

Voegele, A. F., Loerting, T., Tautermann, C. S., Hallbrucker, A., Mayer, E., Liedl, K. R., 2004. Sulfurous acid (H_2SO_3) on Io. Icarus, 169, 242-249, http://doi.org/10.1016/j.icarus.2003.11.012

Voegele, A. F., Tautermann, C. S., Loerting, T., Hallbrucker, A., Mayer, E., Liedl, K. R., 2002. About the stability of sulfurous acid (H_2SO_3) and its dimer. Chem. Eur. J., 8, 5644-5651, http://doi.org/10.1002/chin.200313001

Vogt, R., Crutzen, P. J., Sander, R., 1996. A mechanism for halogen release from sea-salt aerosol in the remote marine boundary layer. Nature, 383, 327-330, http://doi.org/10.1007/978-3-319-27460-7_8

von Glasow, R., Sander, R., Bott, A., Crutzen, P. J., 2002. Modeling halogen chemistry in the marine boundary layer 2. Interactions with sulfur and the cloud-covered MBL. J. Geophys. Res. Atmos., 107, 1-2, http://doi.org/10.1029/2001JD000943

Wang, G., Zhang, R., Gomez, M. E., Yang, L., Levy Zamora, M., Hu, M., Lin, Y., Peng, J., Guo, S., Meng, J., Li, J., Cheng, C., Hu, T., Ren, Y., Wang, Y., Gao, J., Cao, J., An, Z., Zhou, W., Li, G., Wang, J., Tian, P., Marrero-Ortiz, W., Secrest, J., Du, Z., Zheng, J., Shang, D., Zeng, L., Shao, M., Wang, W., Huang, Y., Wang, Y., Zhu, Y., Li, Y., Hu, J., Pan, B., Cai, L., Cheng, Y., Ji, Y., Zhang, F., Rosenfeld, D., Liss, P. S., Duce, R. A., Kolb, C. E., Molina, M. J., 2016. Persistent sulfate formation from London Fog to Chinese haze. P. Natl. Acad. Sci. Usa., 113, 13630-13635, http://doi.org/10.1073/pnas.1616540113

Wang, J., Li, J., Ye, J., Zhao, J., Wu, Y., Hu, J., Liu, D., Nie, D., Shen, F., Huang, X., Huang, D. D., Ji, D., Sun, X., Xu, W., Guo, J., Song, S., Qin, Y., Liu, P., Turner, J. R., Lee, H. C., Hwang, S., Liao, H., Martin, S. T., Zhang, Q., Chen, M., Sun, Y., Ge, X., Jacob, D. J., 2020. Fast sulfate formation from oxidation of SO_2 by NO_2 and HONO observed in Beijing haze. Nat. Commun., 11, 1-7, http://doi.org/10.1038/s41467-020-16683-x

Wang, Y., Zhang, Q., Jiang, J., Zhou, W., Wang, B., He, K., Duan, F., Zhang, Q., Philip, S., Xie, Y., 2014. Enhanced sulfate formation during China's severe winter haze episode in January 2013 missing from current models. J. Geophys. Res. Atmos., 119, 10425-10440, http://doi.org/10.1002/2013JD021426

Wang, Y. H., Liu, Z. R., Zhang, J. K., Hu, B., Ji, D. S., Yu, Y. C., Wang, Y. S., 2015. Aerosol physicochemical properties and implications for visibility during an intense haze episode during winter in Beijing. Atmos. Chem.

Phys., 15, 3205-3215, http://doi.org/10.5194/acp-15-3205-2015

Xu, L., Coote, M. L., 2019. Methods to improve the calculations of SMD solvation free energies and associated aqueous pKa values: comparison between choosing an optimal theoretical level, solute cavity scaling and using explicit solvent molecules. J. Phys. Chem. A, 123, 7430-7438, http://doi.org/10.1021/acs.jpca.9b04920

Yan, J., Jung, J., Lin, Q., Zhang, M., Xu, S., Zhao, S., 2020. Effect of sea ice retreat on marine aerosol emissions in the Southern Ocean, Antarctica. Sci. Total Environ., 745, 140773, http://doi.org/10.1016/j.scitotenv.2020.140773

Zhang, F., Wang, Y., Peng, J., Chen, L., Sun, Y., Duan, L., Ge, X., Li, Y., Zhao, J., Liu, C., Zhang, X., Zhang, G., Pan, Y., Wang, Y., Zhang, A. L., Ji, Y., Wang, G., Hu, M., Molina, M. J., Zhang, R., 2020. An unexpected catalyst dominates formation and radiative forcing of regional haze. P. Natl. Acad. Sci. Usa., 117, 3960-3966, http://doi.org/10.1073/pnas.1919343117

Zhang, H., Wang, W., Pi, S., Liu, L., Li, H., Chen, Y., Zhang, Y., Zhang, X., Li, Z., 2018. Gas phase transformation from organic acid to organic sulfuric anhydride: possibility and atmospheric fate in the initial new particle formation. Chemosphere, 212, 504-512, http://doi.org/10.1016/j.chemosphere.2018.08.074

Zhang, Y., Bao, F., Li, M., Chen, C., Zhao, J., 2019. Nitrate-enhanced oxidation of SO_2 on mineral dust: a vital role of a proton. Environ. Sci. Technol., 53, 10139-10145, http://doi.org/10.1021/acs.est.9b01921

Zhao, J., Kong, X., He, K., Xu, H., Mu, J., 2020. Assessment of the radiation effect of aerosols on maize production in China. Sci. Total Environ., 720, 137567, http://doi.org/10.1016/j.scitotenv.2020.137567

Zhao, Y., Truhlar, D. G., 2008. The M06 suite of density functionals for main group thermochemistry, thermochemical kinetics, noncovalent interactions, excited states, and transition elements: two new functionals and systematic testing of four M06-class functionals and 12 other functionals. Theor. Chem. Acc., 120, 215-241, http://doi.org/10.1007/s00214-007-0310-x

Zheng, B., Zhang, Q., Zhang, Y., He, K. B., Wang, K., Zheng, G. J., Duan, F. K., Ma, Y. L., Kimoto, T., 2015. Heterogeneous chemistry: a mechanism missing in current models to explain secondary inorganic aerosol formation during the January 2013 haze episode in North China. Atmos. Chem. Phys., 15, 2031-2049, http://doi.org/10.5194/acp-15-2031-2015